THE ASTROPHYSICAL JOURNAL, 432:167–180, 1994 September 1

THE COLD, MASSIVE MOLECULAR CLOUD G216−2.5. II. STRUCTURE AND KINEMATICS

YOUNGUNG LEE
Five College Radio Astronomy Observatory and Department of Physics and Astronomy, University of Massachusetts, Amherst, MA 01003; and Korea Astronomy Department, Taejon, Korea 305-348

AND

RONALD L. SNELL AND ROBERT L. DICKMAN[1]
Five College Radio Astronomy Observatory and Department of Physics and Astronomy, University of Massachusetts, Amherst, MA 01003

Received 1993 November 8; accepted 1994 February 28

ABSTRACT

We have studied the gas properties and kinematics of G216−2.5 (also called Maddalena's cloud), a cold, massive giant molecular cloud (GMC) with no obvious signs of star formation. We have mapped 11 square degrees of the cloud in the $J = 1$–0 transitions of ^{12}CO and ^{13}CO using the QUARRY 15 beam array receiver on the 14 m telescope at FCRAO. We confirm the results of Maddalena & Thaddeus (1985) that the cloud is unusually cold and has very broad line widths ($\Delta V \sim 8$ km s^{-1}). The exceptionally low gas temperatures (less than 8 K) can be explained if the cosmic-ray heating rate is reduced by a factor of 2 in the outer Galaxy. The mass of the cloud has been established by several techniques, and masses between 1×10^5 and 6×10^5 $M_\odot$ were obtained.

We suggest that G216−2.5 is a remnant cloud from a past episode of massive star formation, for the following reasons. First, the cloud has a relatively large velocity dispersion for a non–star-forming GMC. Second, there is clear evidence for shells and rings within the cloud, which may be the fossil remains of its earlier star formation activity. Third, the kinematics of the cloud are dominated by a global velocity gradient, suggesting that the cloud is part of a very large expanding shell. Finally, the discrepancy between the LTE and virial masses may be explained if the cloud has been severely perturbed and is currently expanding. G216−2.5 may be part of a larger star-forming complex that includes the adjacent H II region S287 and its molecular cloud.

Subject headings: ISM: individual (G216−2.5) — ISM: kinematics and dynamics — ISM: molecules — radio lines: ISM

1. INTRODUCTION

A large and unusually cold molecular cloud at Galactic coordinates $l = 216.^\circ5$ and $b = -2.^\circ5$ was identified by Maddalena & Thaddeus (1985; hereafter we refer to this object as G216−2.5 or Maddalena's cloud). Maddalena & Thaddeus estimated the cloud to have a mass of approximately 10^6 $M_\odot$ and noted that it lacked all the signs of star formation usually shown by objects of this mass. They also found it to be less fragmented than clouds of similar mass; however, the poor angular resolution of their data prevented them from resolving any small-scale structure within the cloud. Based on these facts, Maddalena & Thaddeus suggested that G216−2.5 was very young and had not yet begun extensively forming stars. Mooney (1992), Solomon, Sanders, & Rivolo (1985), and Myers et al. (1986) have identified many giant molecular clouds (GMCs) with properties similar to G216−2.5; thus, there may be many GMCs without massive star formation. Since G216−2.5 is the nearest example of such objects, it warrants further study.

G216−2.5 has been a subject of two recent molecular line studies by Lee, Snell, & Dickman (1991), and Williams & Blitz (1993). Lee et al. (1991, hereafter Paper I) mapped the core of the cloud in both ^{12}CO and ^{13}CO and determined its visual extinction using star counts. From these data they deduced that the CO abundance for this outer Galaxy GMC is similar to that of clouds near the Sun. They also found that the mass of the cloud core derived from their virial analysis was 5 times greater than the mass estimated assuming LTE. Based on the mass discrepancy and the observed structure and kinematics of the cloud, they suggested that the inner region of the cloud may be expanding. More recently, Williams & Blitz (1993) mapped a small region of the cloud core in ^{13}CO and investigated its structure. They found a rich internal morphology that they characterized in terms of clumps. They found that the clump mass spectrum for G216−2.5 was much flatter than that measured in the Rosette molecular cloud.

Although substantial differences have been found between G216−2.5 and other GMCs of similar mass, the evolutionary state of G216−2.5 is still unclear. Is G216−2.5 a GMC that will never form massive stars, or is it simply very young, as suggested by Maddalena & Thaddeus (1985), and has not had enough time to form massive stars? To further address this issue we have obtained high angular resolution maps of G216−2.5 in ^{12}CO and ^{13}CO covering the entire extent of the cloud in order to determine its global structure, kinematics, and relationship to the nearby star-forming site S287. We use these data to determine the gas temperature, mass, internal structure, and kinematics in an effort to determine the cloud's evolutionary state more securely.

2. OBSERVATIONS

Maps of G216−2.5 were obtained in the $J = 1$–0 transitions of ^{12}CO and ^{13}CO using the QUARRY 15 beam array receiver (Erickson et al. 1992) at the FCRAO 14 m radio telescope between 1991 February and 1992 February. The spectra were spaced by 50″, and covered ∼11 square degrees from $l = 214^\circ$ to $218.^\circ5$, and from $b = -1^\circ$ to $-4.^\circ5$. Each map consists of

[1] Present address: National Science Foundation, Division of Astronomical Sciences, Washington, DC 20550.

57,300 spectra, or 3820 pointings of the 15 beam receiver and telescope. Two filter banks with 32 channels each having frequency resolutions of 250 kHz and 1 MHz were used for each beam. A velocity coverage of 21 km s^{-1} at a resolution of 0.65 km s^{-1} is therefore provided with the 250 kHz filter bank at the frequency of the ^{12}CO $J = 1–0$ line; this is adequate for G216−2.5. The 1 MHz filter bank provided a velocity coverage of 85 km s^{-1} with a resolution of 2.6 km s^{-1}, and was used to check whether emission at other velocities was detectable toward the cloud.

All observations were made by repeatedly switching to one of several reference positions confirmed to have no CO emission. Each reference observation was shared with observations at 4–8 map positions, depending on the sky stability. Calibration was accomplished by frequently observing an ambient temperature load. All antenna temperatures quoted here are corrected for atmospheric extinction and for the forward spillover and scattering losses of the antenna and radome ($\eta_{fss} = 0.7$ at 110–115 GHz), and are therefore on the T_R^* temperature scale defined by Kutner & Ulich (1981). The final average rms noise of the data in T_R^* unit was 0.3 K in ^{12}CO and 0.16 K in ^{13}CO. Maps of the peak antenna temperature in both ^{12}CO and ^{13}CO are shown in Figures 1 and 2. All data for the illustrations were spatially smoothed to a resolution of 120″; however, no velocity smoothing was done. After spatial smoothing, the rms noise was reduced to 0.09 K in the ^{12}CO data and to 0.05 K for ^{13}CO.

Two H II regions lie near G216−2.5: S287 and S286. The velocity of the emission in S287 is $V_{LSR} = 27$ km s^{-1}, essentially the same as that of G216−2.5. The velocity of the emission associated with S286 is $V_{LSR} = 50$ km s^{-1}, much higher than that of G216−2.5 or S287. Since the distance of S286 is estimated to be 4.8 kpc (Blitz, Fich, & Stark 1982)—substantially greater than the distance of G216−2.5 (Paper I)—S286 must lie substantially beyond S287 and G216−2.5, and is unrelated to them.

More extended CO mapping around S287 was conducted to check its possible association with G216−2.5. A 2.4 deg^2 region centered on the position of the H II region ($l = 218.°1$, $b = -0.°4$) was mapped in ^{12}CO $J = 1–0$ with the QUARRY 15 beam array receiver in 1992 June. A 0.8 deg^2 area was also mapped in ^{13}CO $J = 1–0$, which encompasses most of the ^{12}CO emission. The mapping procedure was the same as for G216−2.5. The average rms noise of the data was 0.38 K in ^{12}CO and 0.21 K in ^{13}CO.

The three brightest ^{13}CO emission regions in G216−2.5 were also observed in the $J = 2–1$ transition of CS, the $J = 1–0$ transition of $C^{18}O$, and the $J = 1–0$ transition of HCO^+. Typical system temperatures were 350–500 K, and the average rms noise (T_R^*) of these data was ∼0.07 K. The three regions mapped were a 13′ × 15′ area centered at $l = 216.°75$, $b = -2.°65$, a 4′ × 5′ area centered at $l = 214.°49$, $b = -1.°81$, and a 4′ × 5′ area centered at $l = 216.°79$, $b = -1.°04$. The two smaller regions mapped are associated with *IRAS* point sources 06543−0209 and 06522−0350. CS, $C^{18}O$, and HCO^+ emission was detected in all three regions. The strongest emission in these three transitions was found toward 06543−0209, which had peak intensities of 0.3, 0.3, and 0.7 K (T_R^*) in CS, $C^{18}O$, and HCO^+, respectively. However, in general the emission in these lines was ≤0.3 K (T_R^*).

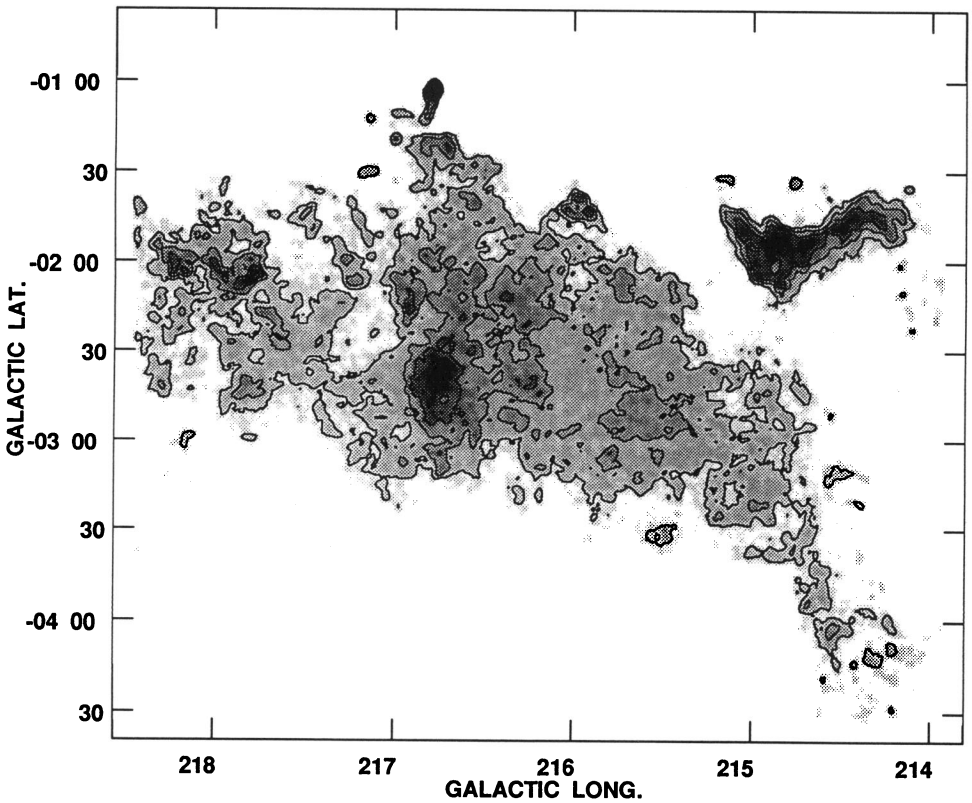

FIG. 1.—^{12}CO peak temperature map of G216−2.5. The gray-scale range is 0.3–3 K, and the lowest contour level and the increments between levels are 0.6 K. The data were spatially smoothed to a resolution of 120″.

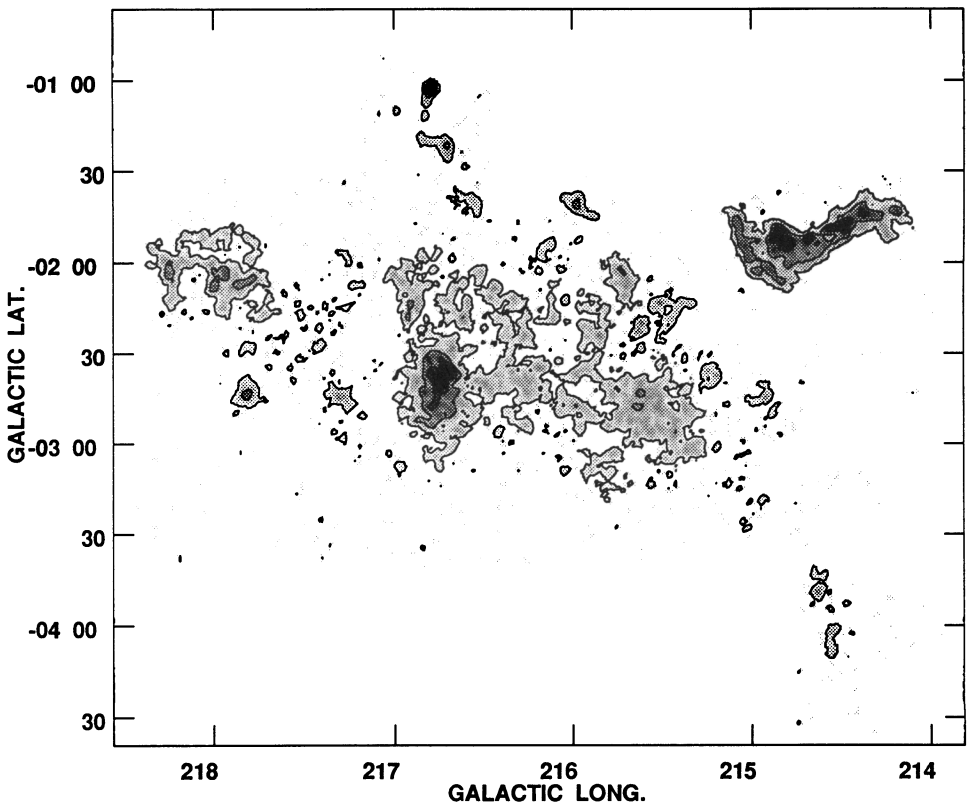

FIG. 2.—^{13}CO peak temperature map of G216−2.5. The gray-scale range is 0.08–1 K, and the lowest contour level and the increments between levels are 0.15 K. The data were spatially smoothed to a resolution of 120″.

3. ANALYSIS

3.1. *Gas Temperature*

Usually the kinetic temperature of a cloud is derived from ^{12}CO observations assuming that the emission is optically thick and thermalized. Maddalena & Thaddeus (1985) originally observed G216−2.5 with the Columbia 1.2 m telescope. Their angular resolution of 8.′7 provided relatively low spatial resolution of 5.5 pc. Thus, even if the cloud filled their beam, the low antenna temperatures that they observed may severely underestimate the temperatures of the warmest regions.

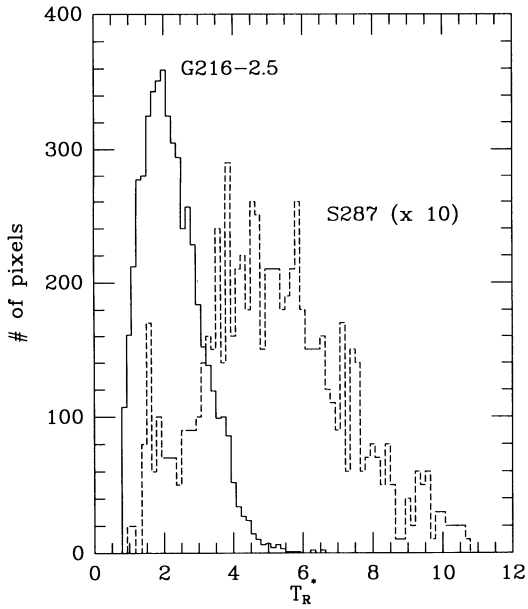

FIG. 3.—Distribution of ^{12}CO peak temperatures in G216−2.5 and S287. All positions with T_R^* (^{13}CO) > 0.5 K are shown. The antenna temperatures are binned in 0.14 K intervals. The numbers of pixels in S287 are multiplied by 10.

The highest antenna temperature in our map is found at the edge of the cloud, in a small knot of emission at $l = 216.°8$ and $b = -1.°06$, and has a peak antenna temperature of $T_R^* = 8.4$ K (see Fig. 1). This is in the direction of an embedded star cluster that will be discussed in a later paper (Lee, Snell, & Dickman 1994, hereafter Paper III). The peak antenna temperature in the main body of G216−2.5 is only $T_R^* = 5.8$ K; however, over most of the cloud, antenna temperatures are less than 4 K and the average T_R^* is 2 K. This is illustrated in the histogram in Figure 3. Clearly, G216−2.5 has substantially weaker CO emission than most GMCs. The ^{13}CO emission strength, on average, is roughly one-tenth that of the ^{12}CO. The peak ^{13}CO antenna temperature is $T_R^* = 4.4$ K and occurs at the same position as the ^{12}CO peak temperature. The highest ^{13}CO antenna temperature in the main body of the cloud is only 2.6 K (Fig. 2).

Radiation temperature is related to corrected antenna temperature by $T_R = T_R^*/\eta_c$, where η_c is the source coupling efficiency. Given the large angular extent of G216−2.5, we have assumed η_c is approximately unity. Thus, assuming optically thick, thermalized emission which fill the antenna beam,

$$T_K = \frac{5.53}{\ln[1 + 5.53/(T_R + 0.876)]} . \quad (1)$$

Since the main body of the cloud has $T_R < 4$ K, the gas temperature is less than 7.3 K.

The assumptions in deriving the gas temperature may be questioned. Non-LTE (NLTE) models of the molecular excitation have been computed to test the validity of the standard LTE assumptions for conditions appropriate to G216−2.5. To include radiative trapping in the excitation calculations, a large velocity gradient (LVG) radiative transfer model was used. For the purposes of checking these assumption, the LVG model is adequate in that it provides a method for solving the statistical equilibrium equations including radiative trapping effects—a feature which may be important for ^{12}CO and which LTE, by definition, cannot address. The CO-H_2 collision rate coefficients used in the model come from Green & Thaddeus (1976), and a diple moment of 0.112 debye was used for CO. The free parameters for the NLTE model are kinetic temperature, density, CO column density, and line width. The velocity width was fixed at 5 km s^{-1}. Thus, the intensities of the lines can be predicted as a function of density and CO column density for a fixed kinetic temperature of 8 K. Densities ranging from 10 to 10^5 cm^{-3} were used, and three ^{13}CO column densities were used (1×10^{16}, 3×10^{15}, and 1×10^{15} cm^{-2}), covering the range of column densities estimated by the LTE technique (see text section). The ^{12}CO column densities were assumed to be 100 times larger.

The model results are presented in Figure 4 and show that the ^{12}CO $J = 1$–0 transition is essentially thermalized and optically thick for densities greater than about 300–1000 cm^{-3}, depending on the CO column density. Moreover, when the ^{13}CO emission is stronger than 0.5 K, it is very likely that ^{12}CO is a good measure of the kinetic temperature. Thus, in directions where strong ^{13}CO emission is observed ($T_R^* > 0.5$ K), equation (1) can in fact be used to estimate the kinetic temperature from the ^{12}CO observations. Note that in the histogram presented in Figure 3, only directions with $T_R^*(^{12}\mathrm{CO}) > 0.5$ K are shown; thus, the gas temperature does appear to be unusually low for this cloud.

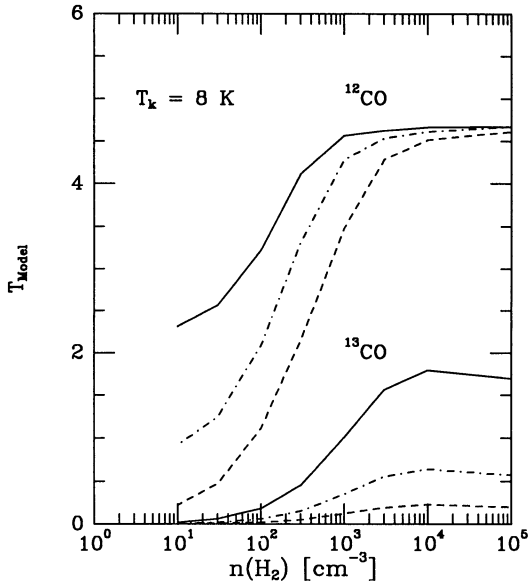

FIG. 4.—NLTE model antenna temperatures for ^{12}CO and ^{13}CO as a function of density for three different column densities. For ^{13}CO the column densities were 1×10^{16} (*solid line*), 3×10^{15} (*dot-dash line*), and 1×10^{15} cm^{-3} (*dashed line*). The ^{12}CO column densities are 100 times larger.

3.2. *Mass of G216−2.5*

3.2.1. *LTE Mass Estimate*

The LTE method has been widely used to estimate cloud masses. A brief discussion of this technique and the assumptions inherent in its use were presented in Paper I. This technique allows the ^{13}CO column density to be derived along lines of sight in which both the ^{12}CO and ^{13}CO lines have been observed. Using the relationship between A_V and ^{13}CO column density from Paper I and the relationship between A_V and total hydrogen column given by Bohlin, Savage, & Drake (1978), the total gas column density can be derived, and subsequently the mass of the cloud. The derived equation for the total gas column density from the ^{13}CO LTE column density can be expressed as

$$N(\mathrm{H\ I}) + 2N(\mathrm{H_2}) = 2 \times 10^{21}\left[\frac{N(^{13}\mathrm{CO})}{1.73 \times 10^{15}} + 0.95\right]. \quad (2)$$

The intercept in the above expression arises from the relation between A_V and ^{13}CO column density and can be understood if G216−2.5 has regions in which either CO is photodissociated or the density is insufficient to excite ^{13}CO emission, but the dust in these regions contributes to the visual extinction. The total mass of G216−2.5, including a factor of 1.36 to account for the contribution of helium by mass, is therefore estimated to be $1.1 \times 10^5\ M_\odot$.

3.2.2. *Virial Mass Estimate*

If a molecular cloud is gravitationally bound and has had enough time to be dynamically relaxed, then the partition of energy will be governed by the virial theorem. The virial mass is given by

$$M_{\mathrm{VIR}} = \frac{3\beta\sigma_{\mathrm{tot}}^2}{2G} D\,, \quad (3)$$

where D is the cloud diameter and σ_{tot} is velocity dispersion of the cloud, which represents all forms of kinetic motion within the cloud. The constant β is order of unity and depends on the shape and density distribution of the cloud. Since clouds are irregularly shaped, it is not straightforward to define a cloud size. We adopt as a measure of the mean cloud diameter $D = (4A/\pi)^{1/2}$, where A is the area. (Here we define the area of the cloud to be that covered by all pixels with ^{12}CO integrated intensity greater than 5 σ.) The size of G216−2.5 is then 100.8 pc, assuming a distance of 2.2 kpc (Paper I).

It is convenient to decompose the gas motions within molecular clouds into two terms which represent two measurable types of motion within the cloud (Dickman & Kleiner 1985). The first is an "internal velocity dispersion," σ_i, which represents the spread of velocities observed along each line of sight, and the second is a "centroid velocity dispersion," σ_c, which is associated with bulk motions of the gas within the cloud that are resolved by the observations. If we assume a uniform density distribution and a spherical cloud ($\beta \sim 1.6$), the virial mass is given by

$$M_{\mathrm{VIR}} = \frac{5\sigma_{\mathrm{tot}}^2}{2G} D\,, \quad (4)$$

where $\sigma_{\mathrm{tot}} = (\sigma_i^2 + \sigma_c^2)^{1/2}$, the one-dimensional velocity disper-

sion. If D is measured in parsecs and σ_{tot} in kilometers per second, we get

$$M_{VIR} = 582 D \sigma_{tot}^2 \, M_\odot \, . \quad (5)$$

The internal and centroid dispersions for G216−2.5 are estimated to be $\sigma_i = 1.82$ km s^{-1}, $\sigma_c = 2.75$ km s^{-1}. Thus, the total velocity dispersion, σ_{tot}, is 3.29 km s^{-1}, which corresponds to $\Delta V = 7.75$ km s^{-1}. From equation (5), a virial mass of $6.36 \times 10^5 \, M_\odot$ is therefore obtained for G216−2.5.

3.2.3. *Mass from the CO Luminosity*

Another mass estimate can be obtained by using the empirical relationship between the CO integrated intensity and molecular hydrogen column density or, equivalently, the relationship between CO luminosity and mass. This relationship has been studied by a number of investigators and reviewed by Scoville & Sanders (1987). Usually the virial mass is used to calculate the conversion factor. In fact, if clouds are virialized, a relation between total CO luminosity and cloud mass can be theoretically demonstrated to exist (Dickman, Snell, & Schloerb 1986). Empirical estimates of the conversion constant based on molecular observations vary in the range $(1–5) \times 10^{20}$ cm^{-2} (K km s^{-1})$^{-1}$ (Scoville & Sanders 1987); the lack of agreement for this quantity is the dominant source of uncertainty in deriving molecular gas masses by this method.

The conversion factor has also been established through γ-ray analysis. Several γ-ray studies (Lebrun et al. 1983; Bloemen et al. 1984; and summary by Bloemen 1989) found similar conversion constants in the range $(2–3) \times 10^{20}$ cm^{-2} (K km s^{-1})$^{-1}$. Also, the γ-ray analysis suggests that the conversion factor is roughly constant as a function of Galactic radius, except possibly for the center of the Galaxy (Bloemen 1987). One merit of this method for determining the conversion function is that it is independent of virial mass estimates; the γ-ray flux directly probes the hydrogen column density.

The ^{12}CO luminosity of G216−2.5 is 6.1×10^4 K km s^{-1}. Thus, if we use the most recent estimate of the conversion factor, 2.3×10^{20} cm^{-2} (K km s^{-1})$^{-1}$ (Bloemen 1989), we obtain a mass of $3 \times 10^5 \, M_\odot$.

3.3. *Cloud Density*

With some assumptions about geometry, the average spatial density can be computed using the mass estimates presented in the previous section. We assume the cloud is a cylinder 100 pc in length and 50 pc in diameter. With a mass between 10^5 and $6 \times 10^5 \, M_\odot$, the average density of the cloud is then between 10 and 60 cm^{-3}. This is much lower than that of most GMCs, which have average densities of a few hundred cm^{-3} (Solomon et al. 1987). However, while the average density based on global cloud properties is useful, it may be far from giving a reasonably accurate picture of the density in an inhomogeneous molecular cloud.

Another method of estimating the density is based on measurements of column density and estimates of line-of-sight distances. The highest ^{13}CO column density in G216−2.5 is approximately 10^{16} cm^{-2}; thus, the total H_2 column density is roughly 6×10^{21} cm^{-2}. The high column density region has an angular size of $\sim 0.^\circ 1$; if it is spherical, then the line-of-sight distance is approximately 3.8 pc. The average density along this line of sight is thus roughly 500 cm^{-3}. However, our models (§ 3.1) indicate that densities of 500 cm^{-3} are insufficient to explain the strength of the observed ^{13}CO emission. Thus, the cloud must be inhomogeneous on size scales less than 4 pc.

The CS emission provides an additional constraint on the density within the cloud. A contour map of the CS emission centered on $l = 216.^\circ 75$, $b = 2.^\circ 65$ is presented in Figure 5. At least two elongated, clumpy structures are observed, reinforcing the idea that the density structure within G216−2.5 is very inhomogeneous. The observed antenna temperatures in this large region and in the two smaller regions mapped in CS are about 0.3 K. Assuming a kinetic temperature of 8 K, a relative CS abundance of 10^{-8}, and a line width of 3 km s^{-1}, a density of $\geq 3 \times 10^3$ cm^{-3} is required to match the observations.

The CS emission associated with the two *IRAS* sources is much smaller in extent than that in the region shown in Figure 5; the extent of the CS emission in 06453−0209 is 0.5 pc, and the extent of the CS emission in 06522−0350 is 0.3 pc. Assuming that the CS emission is optically thin and has an excitation temperature of 10 K, and that the CS abundance is 1×10^{-8}, the mass of the core in 06453−0209 is 23 $M_\odot$ and the mass of the core in 06522−0350 is 10 $M_\odot$. Thus, the large (a few parsecs) and massive (100–1000 $M_\odot$) cores found in most GMCs (Goldsmith 1988) are absent in G216−2.5. The cores identified in G216−2.5 have sizes, characteristic CS temperatures, and masses more typical of those found in dark clouds (Goldsmith 1988).

3.4. *Morphology and Velocity Structure*

G216−2.5 has a extent of $4.^\circ 5$ in Galactic longitude, and $2.^\circ 5$ in Galactic latitude, centered on $l = 216.^\circ 5$, $b = -2.^\circ 5$. Assuming a distance of 2.2 kpc, the full extent of the cloud is 170 × 100 pc (see Fig. 1). This is larger than the average GMC (Goldsmith 1988; Solomon et al. 1987).

G216−2.5 is comprised of an elongated main cloud and a smaller satellite cloud about one-fifth the size of the main cloud. The companion is located just $0.^\circ 5$ from the border of the main cloud, and has similar properties. Both clouds are very cold, as originally pointed by Maddalena & Thaddeus (1985), and have the same mean velocity of $V_{LSR} = 27$ km s^{-1}. Thus, they are almost certainly associated.

Maps of both clouds at individual velocities are shown in Figure 6. Two spectrometer channels were binned together for each map (the velocity resolution per channel is 0.65 km s^{-1}, so that the velocity coverage of each map is 1.3 km s^{-1}), and the velocity range covered by the maps is 18–34 km s^{-1}. The maps reveal a rather complicated velocity structure. The most striking features are an oval-shaped structure seen in Figures 6*a*–6*c* and a ringlike structure seen in Figures 6*g*–6*i* centered at $l = 216.^\circ 7$, $b = -2.^\circ 2$. The ring is almost 50 pc in diameter at $V_{LSR} = 27$ km s^{-1}; at higher velocities it is much larger, and the emission is found preferentially on the left-hand side (higher Galactic longitude) of the ring.

In Figure 7 we present a series of latitude-velocity maps at $l = 217.^\circ 2$, $216.^\circ 88$, and $216.^\circ 55$ with a velocity coverage of 16–38 km s^{-1}, running from left to right. The locations of the position-velocity maps are indicated by the vertical lines in Figure 8. The three position-velocity maps highlight the velocity structure near the ringlike feature at $l = 217.^\circ 7$ and $b = -2.^\circ 2$ that was noted above. The center position-velocity map in Figure 7 cuts through the center of the ring, and the emission from the ring splits into blueshifted and redshifted components, while the position-velocity maps that pass through the edges of the ring (the left- and right-hand plots in Fig. 7)

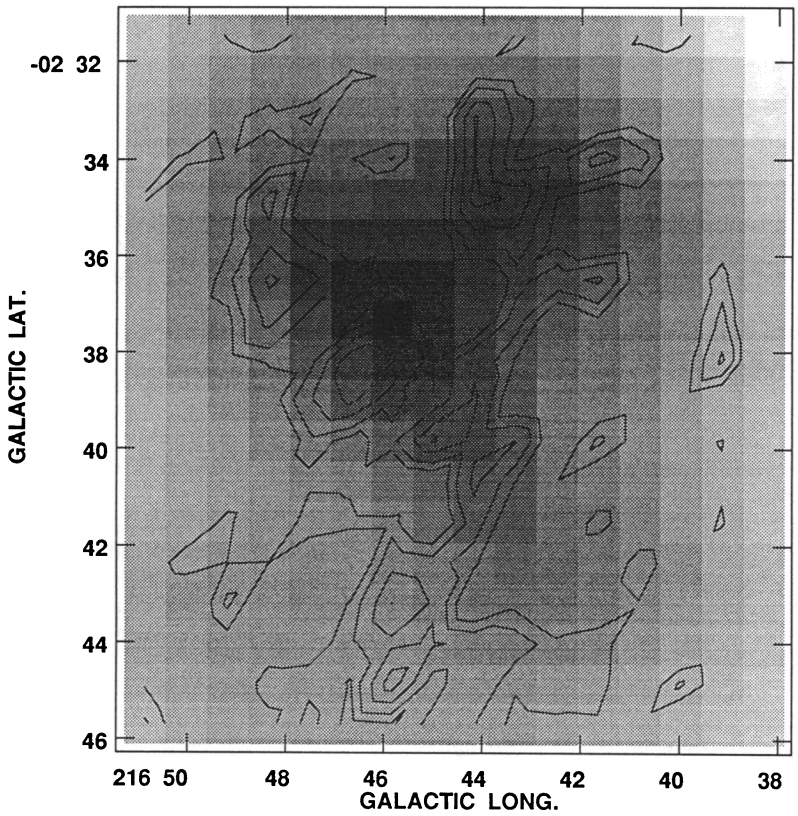

FIG. 5.—Contour map of CS peak antenna temperature overlaid on a gray-scale image of the ^{13}CO integrated intensity. The range of the gray-scale image is 0.5–3.15 K km s^{-1}, the lowest contour level is 0.12 K, and the interval between contours is 0.05 K.

show only a single velocity component of intermediate velocity relative to the blueshifted and redshifted components. Thus, the velocity pattern matches what would be expected for an expanding shell. The angular size of this shell is about 0°.5, or a linear size of 20 pc, and the expansion velocity is a few km s^{-1}, thus suggesting a dynamical age of about 3×10^6 yr.

The position-velocity maps presented in Figure 7 also show that there is substantial systematic velocity structure within the cloud. This structure is more obvious in the position-velocity map shown in Figure 9 made diagonally across the cloud from $l = 217°.7$, $b = -3°.4$ to $l = 215°.4$, $b = -1°.8$ (the location is indicated in Fig. 8). The velocity difference between the center and edge of the cloud along this direction is 10 km s^{-1}. A map of the mean velocity of the cloud is shown in Figure 10 and demonstrates that the cloud has a global velocity pattern in which the largest blueshifted velocities are found at the center of the cloud, while at the edges the gas is relatively more redshifted. One possible explanation for this systematic velocity structure is that the cloud forms the front portion of a large expanding shell. If this model is correct, the shell diameter would have to be greater than 120 pc and its expansion velocity at least 5 km s^{-1}. In any case, the global velocity structure of G216−2.5 is clearly dominated by large-scale motion; it appears that the cloud is a remnant of a severely disrupted progenitor. The broad line widths that we see may be largely due to unresolved systematic motions.

3.5. *S287 and Its Associated Molecular Cloud*

The H II region S287 and its associated molecular cloud are located at $l = 218°.1$, $b = -0°.4$. Their projected distance from the center of G216−2.5 is only 100 pc. The ^{12}CO peak temperature is 12 K, and the ^{13}CO peak temperature is 5 K. In Figure 11 a ^{12}CO integrated intensity map of the S287 cloud along with G216–2.5 is shown. The morphology of the cloud is quite different from that of G216−2.5, consisting of two major concentrations of gas connected by a long filament. S287 is associated with the left-hand (higher Galactic longitude) concentration of gas (the location is marked by a filled triangle in Fig. 12); this H II region is excited by an O9.5 star (Moffat, Fitzgerald, & Jackson 1979). Located toward the right-hand concentration of gas at $l = 217°.4$, $b = -0°.1$ is the bipolar nebula NS 14. Neckel et al. (1989) found four stars of spectral type B0.5–A5 associated with this bipolar nebula that are deeply embedded within the dense molecular cloud. Thus, in contrast to the case of G216−2.5, there are several sites of massive star formation within this cloud. Its filamentary structure is probably being shaped by the strong stellar winds from these young stars. The mass of the S287 cloud also has been estimated by both the LTE and the virial methods. The virial mass estimate is $6 \times 10^4\ M_\odot$ (287 has a size of 26 pc, and a line width of 4.5 km s^{-1}), and the LTE mass estimate is $1.3 \times 10^4\ M_\odot$.

4. DISCUSSION

4.1. *Gas Temperatures*

Perhaps the most noteworthy feature of G216−2.5 is that ^{12}CO radiation temperatures are much lower than in normal GMCs (Fig. 3). The average peak temperature is only ~2 K for G216−2.5, while for S287 the average is 5.5 K. The maximum ^{12}CO antenna temperature found in the main body of the cloud is 5.8 K. This translates into a gas kinetic temperature of

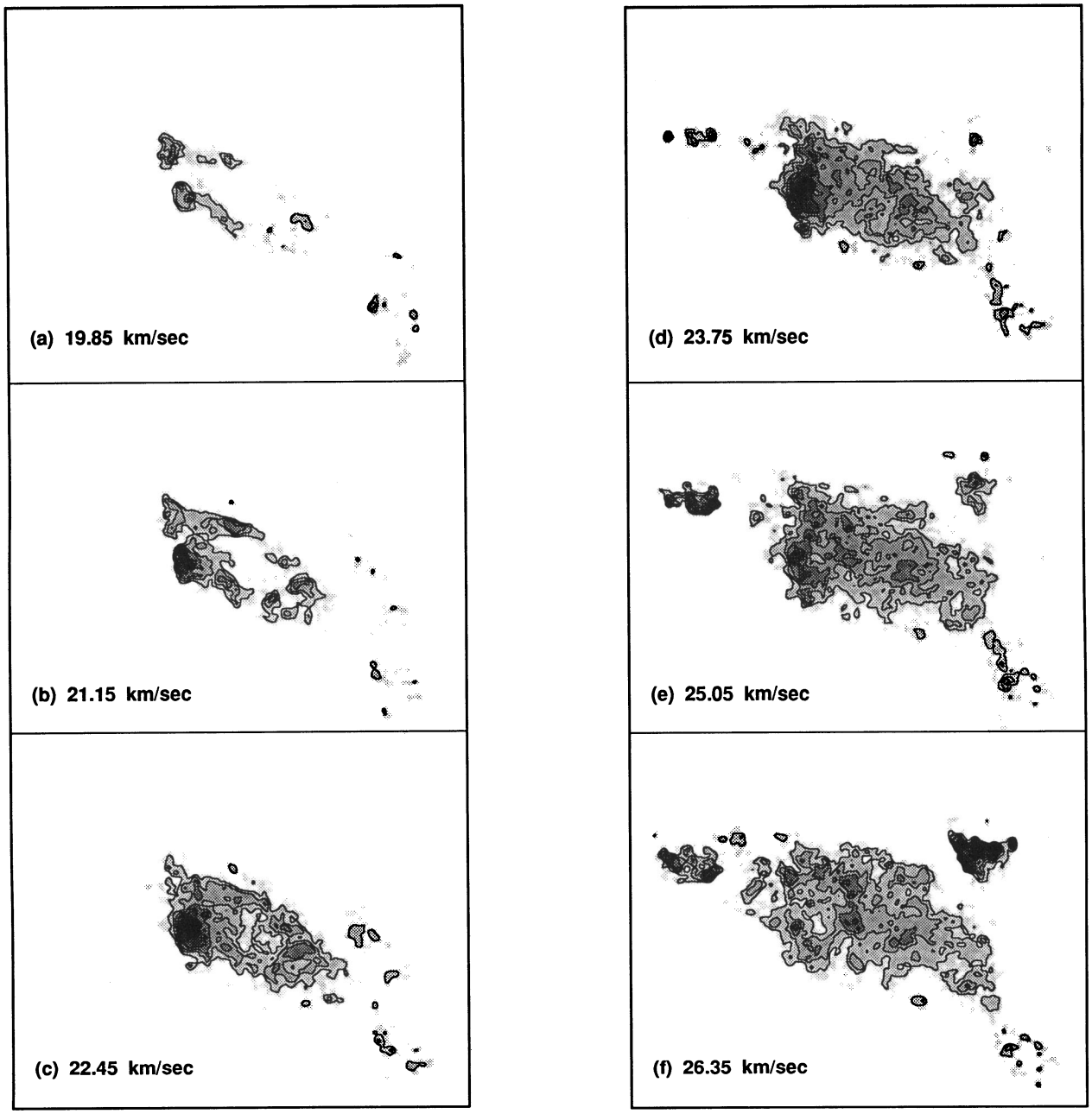

FIG. 6.—(*a–l*) ^{12}CO velocity maps of G216−2.5 with 50″ resolution. Two velocity channels are binned together in each map; thus, each map has V_{LSR} range of 1.3 km s^{-1}, centered at a V_{LSR} of 19.85 (*a*), 21.15 (*b*), 22.45 (*c*), 23.75 (*d*), 25.05 (*e*), 26.35 (*f*), 27.65 (*g*), 28.95 (*h*), 30.25 (*i*), 31.55 (*j*), 32.85 (*k*), and 34.15 (*l*) km s^{-1}.

8.3 K, at the low end of temperatures found typically in dark clouds of 8–13 K (Dickman 1978; Snell 1981). Why is the gas in G216−2.5 so cold? First and foremost, G216−2.5 has no luminous internal heating sources; the closest OB associations are more than 500 pc from G216−2.5 (Lee 1992), and the closest OB stars are found in S287, at a distance of at least 100 pc. Thus, direct heating of G216−2.5 by stars in S287 is very small.

In the absence of embedded stellar heating sources, the primary heating mechanism for the gas is cosmic rays. This remains true even if the interstellar radiation field plays an important role in heating the dust, since the density of G216−2.5 is not sufficient to couple the dust and gas temperatures, except perhaps in the denser regions of the cloud where $n(H_2) > 10^4$ cm^{-3}.

The temperature of the gas in G216−2.5 is therefore probably established by the balance between cosmic-ray heating and gas radiative cooling. Goldsmith & Langer (1978) have shown that for the densities relevant for the bulk of G216−2.5, the cooling of the gas is dominated by the emission of CO and its isotopic variants ^{13}CO and C^{18}O. To determine the precise rate at which this energy is radiated from the cloud requires a model for the radiative transfer. However, for nearly thermalized and optically thick transitions, such as ^{12}CO, the cooling per molecule is relativey independent of the molecular abundance and the density of the cloud; once the opacity becomes

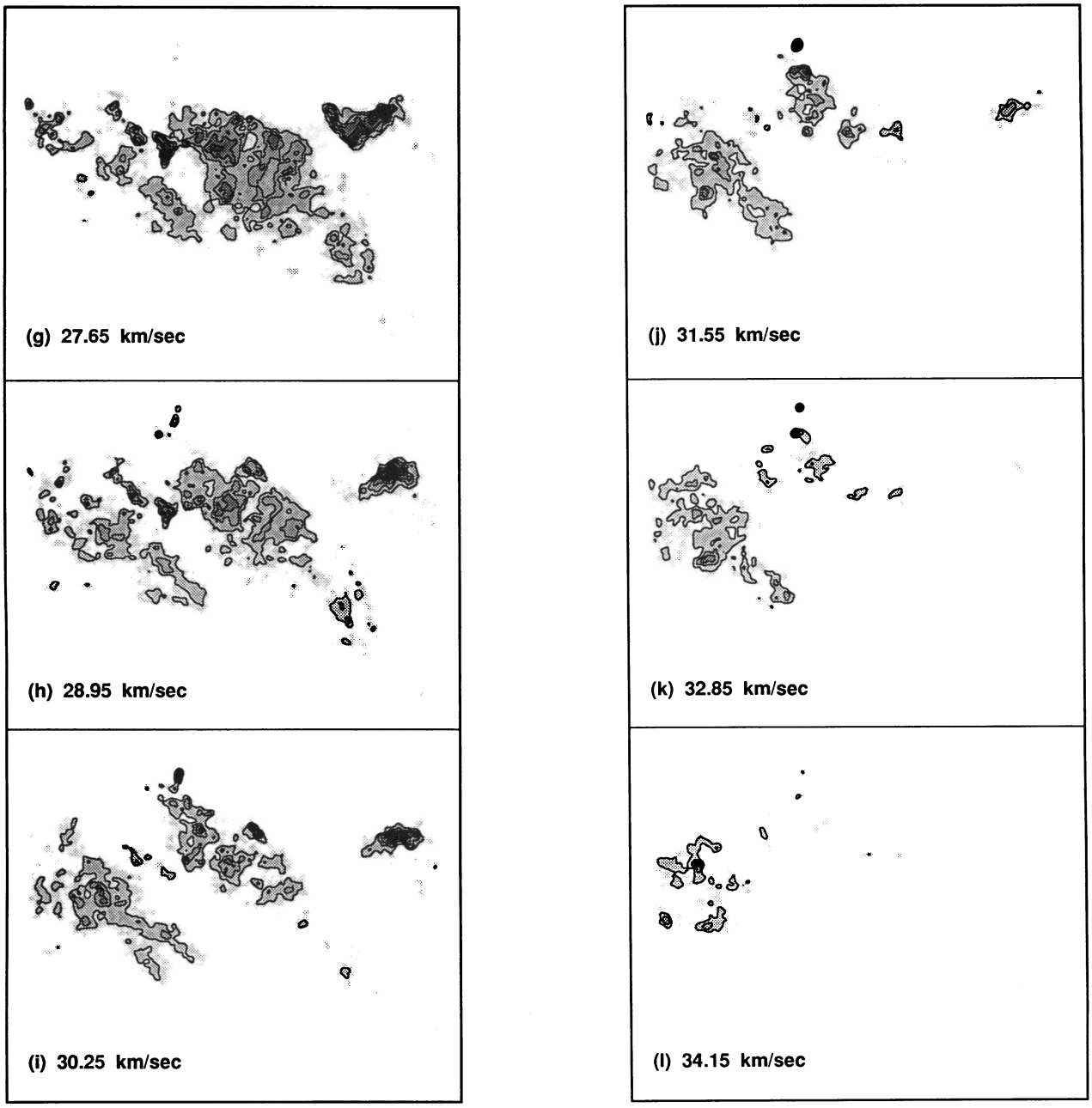

FIG. 6—*Continued*

large, the cooling must be that of a blackbody, thus depending only on the line width and temperature. We adopt the cooling rates given by Goldsmith & Langer (1978).

Goldsmith & Langer (1978) adopted a local cosmic-ray heating rate of $\Gamma_{CR} = 6.4 \times 10^{-28}\, n(H_2)$. However, it has been suggested that the cosmic-ray flux may be reduced in the outer Galaxy (see Dodds, Strong, & Wolfendale 1975; Higdon 1979; review by Bloemen 1989). Thus, we have considered two cosmic-ray heating rates: that given by Goldsmith & Langer and one reduced by a factor of 2. Balancing the heating and cooling rates, we can solve for the temperature as a function of density. The results are shown in Figure 13.

Modeling of the ^{13}CO emission in G216−2.5 suggests that the density has to be at least 10^3 cm^{-3}; however, the weak CS emission suggests that the density is unlikely to be much greater than 10^4 cm^{-3}. For the Goldsmith & Langer rate in this density range the gas kinetic temperature is 8–10 K. This range of temperatures agrees very well with the temperatures found in dark clouds in the solar neighborhood (Dickman 1978; Snell 1981). Using the reduced heating rate, the gas kinetic temperature is ~6 K at the same density, which agrees well with the observational results for G216−2.5. Thus, the exceptionally low gas temperatures of G216−2.5 may be explained if the cosmic-ray flux is assumed to be reduced by only a factor of 2 at 2 kpc beyond the solar circle.

This conclusion agrees with previous studies of other outer Galaxy clouds by Mead & Kutner (1988), who noted a prevalence of low cloud temperatures there, and who also suggested

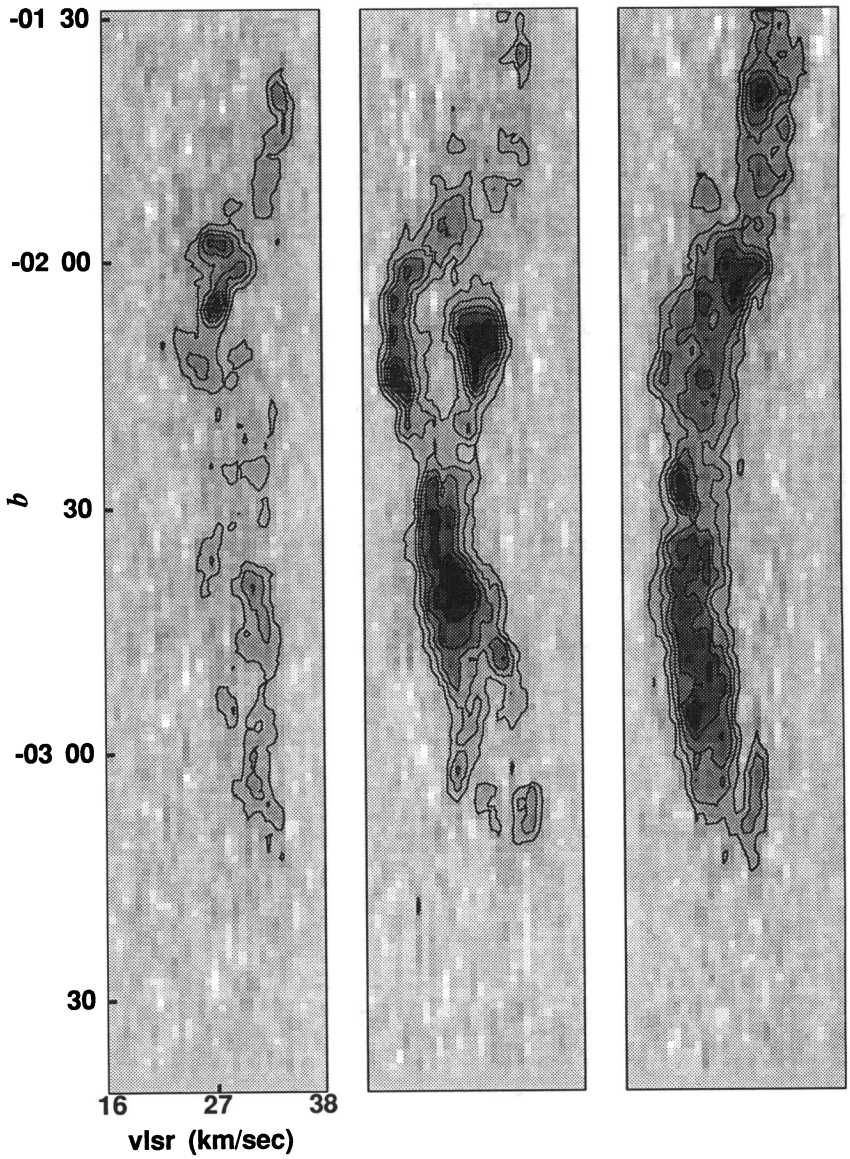

FIG. 7.—Latitude-velocity maps at three different Galactic longitudes, 217°.2 (*left*), 216°.88 (*center*), and 216°.55 (*right*). The lowest contour level and the increments between the contours are 0.25 K. The velocity range of each map is 16–38 km s^{-1} from left to right.

that a factor of 2 decrease in the cosmic-ray heating rate would explain this result.

4.2. *Cloud Mass*

In § 3.2 we presented three different methods for estimating the mass of G216−2.5. The LTE estimate, $1 \times 10^5\ M_\odot$, was the smallest, and the virial estimate, $6 \times 10^5\ M_\odot$, was the largest. In this section we discuss the uncertainties in these mass estimates.

4.2.1. *LTE Mass Estimate*

One of the critical assumptions in the LTE method is that ^{12}CO and ^{13}CO have equal excitation temperatures. We can check the extent to which violations of this assumption affect derived column densities by using the NLTE model described in § 3.1: the model was used to predict isotopic emission intensities over a wide range of densities and CO column densities. The predicted radiation temperatures were than analyzed using the LTE technique to determine how successfully the method recovered the original model column density. Figure 14 shows the ratio of LTE-derived ^{13}CO column density to the original model column density as a function of density. It is clear that for densities less than 3000 cm^{-3}, the column density can be severely underestimated using the LTE technique. Further, as discussed in § 3.3, the volume density of the cloud may be substantially less than 3000 cm^{-3} depending on how inhomogeneous the cloud is on small size scales. Thus, the LTE-derived mass may seriously underestimate the true mass of G216−2.5.

However, a test of the LTE technique was provided in Paper I, in which the visual extinctions determined from star counts and LTE column densities were compared for the central portion of the cloud. A good correlation was found between these two quantities, demonstrating that the LTE column density traces the column density of the cloud material as well as the dust extinction. In fact, both the slope and the intercept

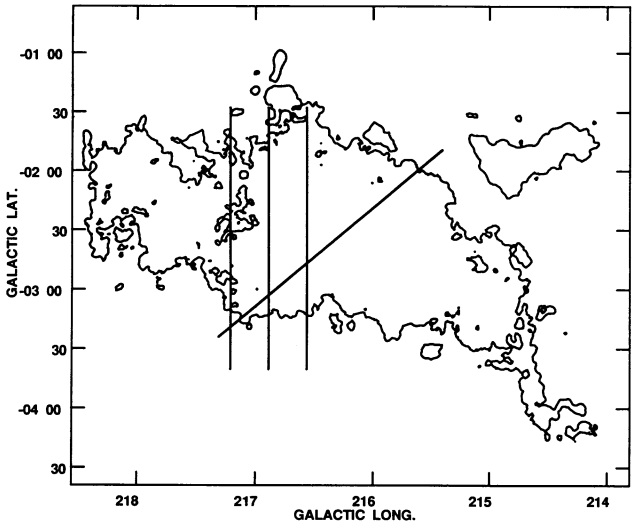

FIG. 8.—Locations of the position-velocity maps overlaid on 5 σ contour of ^{12}CO integrated intensity. The three vertical solid lines show the locations of position-velocity maps presented in Fig. 7. The diagonal line gives the location of the position-velocity map shown in Fig. 9.

found for the relationship between ^{13}CO column density and visual extinction was similar to that found for clouds near the Sun, implying that if the gas-to-dust ratio is normal, then the CO abundance is also similar to that in cloud near the Sun. Thus, if the central portion of the cloud is representative of entire cloud, only if the gas-to-dust ratio is abnormal can the LTE gas column densities and cloud mass derived for G216−2.5 be grossly in error.

More likely sources of error in the LTE mass arise from errors in estimating the visual extinctions and in applying a "universal" extinction to gas column density ratio. While a correlation between proton column density and extinction was empirically established by Bohlin et al. (1978), it was only established for $A_V < 2$ mag. Thus, it is necessary to extrapolate the relation they found in order to apply it to molecular clouds, implicitly assuming that the grain properties are the same as in lower density regions; in fact, there is some evidence that this is not the case, although under conditions pertaining to the bulk of G216−2.5 this is not likely to be an important effect. There are also restrictions on the use of star counts: above $A_V = 5$ mag, it is very difficult to determine the visual extinction

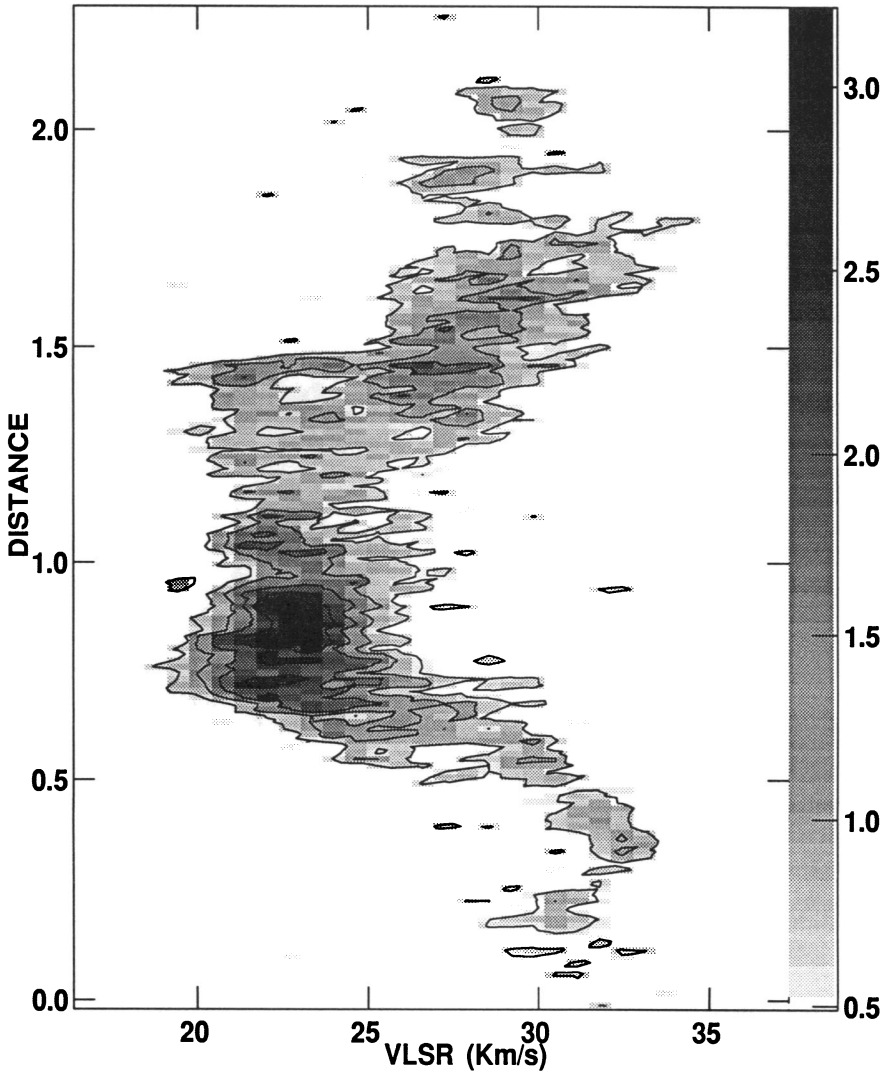

FIG. 9.—^{12}CO position-velocity map for the diagonal cut across the main body of G216−2.5. The velocity range is 16–38 km s^{-1}, and the position goes from $l = 217°.3$, $b = -3°.4$ (*bottom*) to $l = 215°.4$, $b = -1°.8$ (*top*). The lowest contour and the increments between contours are 0.6 K.

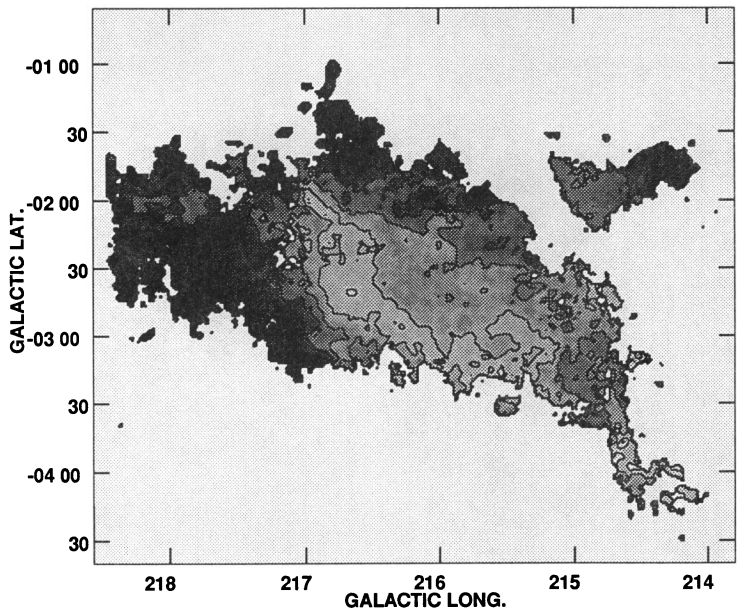

FIG. 10.—Mean ^{12}CO velocity map. The mean velocity is computed only for the regions where the integrated intensity is greater than 5 σ. Darker colors represent higher velocities, and the contour levels span the velocity range 18–34 km s^{-1} in 2 km s^{-1} increments.

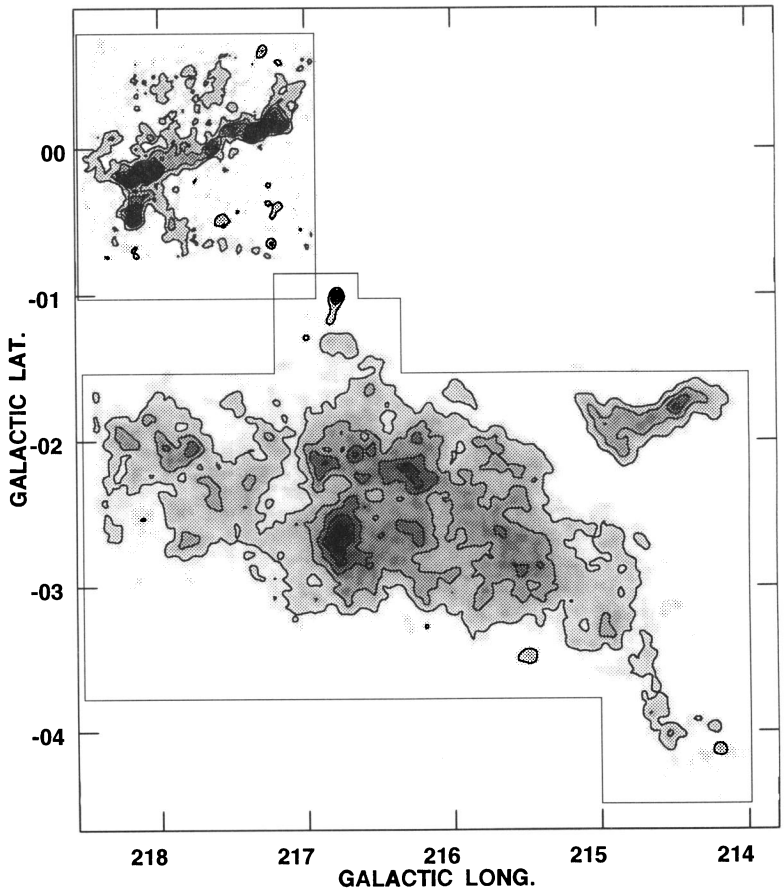

FIG. 11.—^{12}CO integrated intensity map of S287 and G216−2.5. The gray scale covers a range of 0.5–16 K km s^{-1}. The lowest contour level is 2 K km s^{-1}, and the increments between contours are 3 K km s^{-1}.

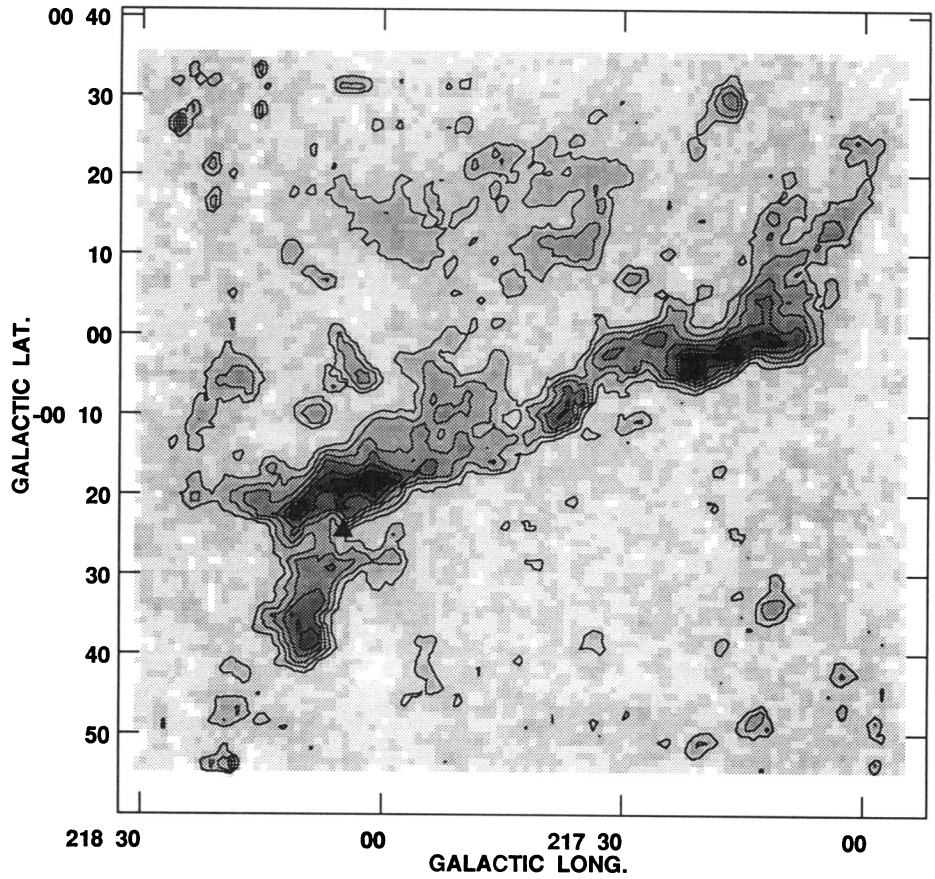

FIG. 12.—^{12}CO peak temperature map of the molecular cloud associated with the H II region S287. The location of the H II region is marked by the filled triangle at $l = 218°.1, b = -0°.4$. The gray scale stretches from 0 to 8 K. The contour levels cover the range from 1 to 10 K in 1 K increments.

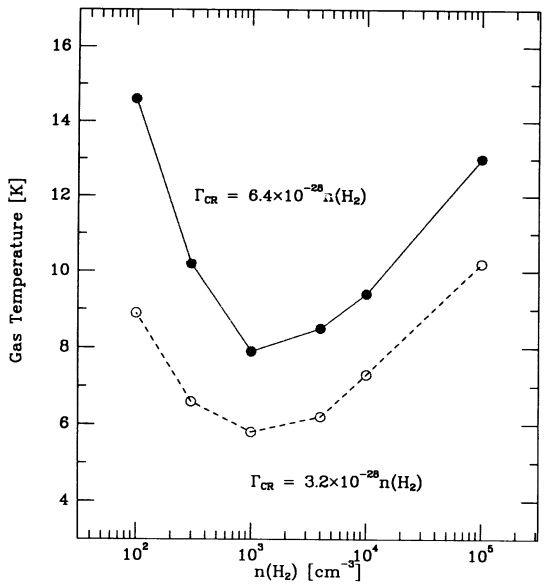

FIG. 13.—Equilibrium gas kinetic temperature as a function of density for two different cosmic-ray heating rates.

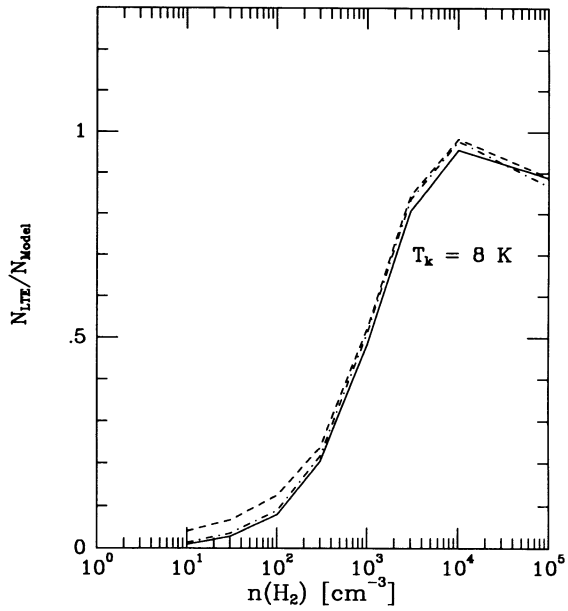

FIG. 14.—Ratio of LTE ^{13}CO column density to model ^{13}CO column density as a function of density. The ratio was calculated for the same column densities as shown in Fig. 4.

because of the small number of stars. However, since the visual extinction for only a small portion of G216−2.5 is greater than 4 mag, our extinction measurements should be generally applicable. Thus, we believe that the LTE mass estimate for G216−2.5 is reliable.

4.2.2. *Virial Mass Estimate*

A number of assumptions enter into the determination of the virial mass, such as the definition of cloud size, the density structure, and the effect of saturation broadening of the ^{12}CO line widths. Any one of these could significantly affect the virial mass estimate. Saturation broadening was discussed in detail in Paper I. Since the centroid velocity dispersion, which is not subject to saturation corrections, contributes a significant fraction of the total velocity dispersion in G216−2.5, the effects of saturation should be minimal.

Size is another parameter that enters the virial mass estimate. We have adopted the mean cloud diameter based on the total area of the cloud. However, this size definition depends on the sensitivity of the CO observations. If the data were less positive, the cloud would appear smaller, whereas if the data were more sensitive, the cloud would appear larger. To avoid this problem, other definitions of cloud size have been used. Solomon et al. (1987) and Carpenter, Snell, & Schloerb (1990) based the size of the cloud on the intensity-weighted dispersions in the two spatial coordinates of their maps.

For a cloud with a fairly uniform emission distribution, the difference between these size definitions and ours is very small. But for a very filamentary, fragmentary, or elongated cloud, the difference can be large as a factor of 2. For an elongated cloud, such as G216−2.5, using the definition of Carpenter et al. (1990) leads to a diameter of 70 pc, a value 30% smaller than our estimate. While a 30% smaller size leads to a 30% smaller virial mass, this does not explain the factor of 6 discrepancy with the LTE mass estimate.

The virial mass also depends on the assumed density distribution of the cloud. For a spherical cloud with a r^{-1} density distribution, the derived virial mass will be 20% larger than that given by equation (5). The constant in equation (5), which is 582, is generally related to the assumed density distribution; Langer, Wilson, & Goldsmith (1989) used 640, while Scoville et al. (1987) used 698. However, these are all within $\pm 20\%$ of the value assumed here, and are therefore likewise not different enough to account for the mass discrepancy.

4.2.3. *Mass Estimate Using Conversion Factor from Gamma-Ray Analysis*

The conversion factor in the CO luminosity-mass relation has been established through γ-ray analysis. We have used a recent estimate of the conversion factor of 2.3×10^{20} cm^{-3} (K km s^{-1})$^{-1}$ (Bloemen 1989), and obtained a mass of 3×10^5 $M_\odot$, although conversion constants in the range (2–3) $\times 10^{20}$ cm^{-2} (K km s^{-1}) have been found (Lebrun et al. 1993; Bloemen et al. 1984; and summary by Bloemen 1989). However, one may still have reasons to be concerned about this estimate. The existence of a general relation between mass and CO luminosity may be the result of most clouds being in virial equilibrium. If G216−2.5 is not in virial equilibrium, its mass could be overestimated by this technique.

4.2.4. *Summary of Mass Estimates*

A factor of 2 or even 3 difference between mass estimates could easily be attributed to a combination of the uncertainties mentioned above. However, the factor of 6 difference found for G216−2.5 is uncomfortably large and may arise because the cloud is not in virial equilibrium. To explore this issue, the kinematics of G216−2.5 are discussed further in the next section.

4.3. *Evolutionary Status of G216−2.5*

G216−2.5 has a striking velocity structure. Rings and an expanding shell-structure appear to be present both in the maps at different velocities and in position-velocity maps. The features are similar to those found in active star-forming clouds. However, in such clouds (e.g., Gem OB1; Carpenter, Snell, & Schloerb 1992) there are usually obvious stellar sources to drive the expanding shells and to generate the rich structure observed. For example, one of the Gem OB1 molecular clouds at $\alpha = 05^h57^m$, $\delta = +20°$ (hereafter Gem OB1-arc) has morphological and kinematic properties very similar to those of G216−2.5. However, it is clearly part of a much larger arc (radius $\sim$120 pc) of molecular gas that encircles the S252/S247 star-forming regions. Using data kindly provided by J. Carpenter for this region, we have estimated LTE and virial masses in the same way as for G216−2.5; the virial mass derived is $M_{\rm VIR} = 6 \times 10^5$ $M_\odot$, and the LTE mass derived is $M_{\rm LTE} = 8 \times 10^4$ $M_\odot$. The mass estimates are similar to those for G216−2.5, as is the discrepancy between the two estimates. Like G216−2.5, Gem OB1-arc also possesses broad line widths, very low gas temperatures, and a total absence of massive star formation. The distribution of peak antenna temperatures is also surprisingly similar to that of G216−2.5. Thus, G216−2.5 and Gem OB1-arc appear to be near-twin clouds. However, it is clear in the case of Gem OB1-arc that it is part of a large shell structure, surrounding still active star-forming sites. While the nearby S287 cloud has associated massive star formation, there is no apparent gas connection between the two clouds: the region between the two clouds was observed in ^{12}CO with 15′ sampling (though this does not completely rule out a thin or lower density gas bridge between the two clouds). One may wonder whether the association between G216−2.5 and S287 is similar to that of Gem OB1-arc and S252/S247.

What is the evolutionary status of G216−2.5? Maddalena & Thaddeus (1985) suggested, based on the absence of massive star formation and its very low temperature, that G216−2.5 was relatively young and had not yet evolved to the point of star formation. Similar suggestions were made by Blitz (1991). However, if GMCs are long-lived, they may undergo episodic massive star formation events. Mooney (1992) describes a scenario in which GMCs undergo a massive star formation burst, fragment and expand, and then appear as quiescent cold clouds, with the fossil remains of the past burst of star formation.

A number of facts about G216−2.5 favor an evolutionary state between episodes of massive star formation. First, the cloud has a relatively large velocity dispersion for a non–star-forming GMC, just what one might expect of the aftermath of a star formation burst. Second, there is clear evidence for shells and rings within the cloud, which may be the fossil remains of earlier star formation activity. Third, the kinematics of the cloud are dominated by a global velocity gradient, consistent with the cloud being part of a very large, mostly dispersed expanding shell. Fourth, the discrepancy between the LTE and virial masses may be explained if the cloud has been severely perturbed and is currently expanding. Finally, the striking morphological and kinematic similarities between G216−2.5

and Gem OB1-arc suggest that both clouds are in similar evolutionary states; for Gem OB1-arc the evidence that it is part of a shell produced by the past star formation activity is much more compelling. Thus, we believe that G216−2.5 is a remnant cloud from an older star formation event. The still active S287 cloud and another nearby cloud mapped by Maddalena & Thaddeus (1985) may all have been part of the molecular cloud complex that included G216−2.5.

5. CONCLUSIONS

We have mapped G216−2.5 in the emission of the $J = 1$–0 transitions of ^{12}CO and ^{13}CO using FCRAO's QUARRY 15 beam array receiver. Each map contains 57,300 spectra covering a region 11 square degrees in extent, with the observations spaced by 50″. As originally pointed out by Maddalena & Thaddeus (1985), we confirm that the cloud has unusually weak emission lines and has very broad line widths ($\Delta V \sim 8$ km s^{-1}).

The CO observations confirm the low gas kinetic temperature found by Maddalena & Thaddeus (1985). The gas heating in G216−2.5 appears to be dominated by cosmic rays, and the low temperature of the cloud can be explained if the cosmic-ray flux in the outer Galaxy is smaller by a factor of ~ 2 than in the solar neighborhood.

The LTE mass of G216−2.5 is estimated to be 1.1×10^5 $M_\odot$, and the virial mass is estimated to be 6.3×10^5 $M_\odot$. The factor of 6 discrepancy between the two mass estimates is larger than expected based on the uncertainties in these methods. The large virial mass may reflect the fact that G216−2.5 is not gravitationally bound.

The average density of G216−2.5 is 10–60 cm^{-3}, much lower than that of most GMCs. Models of the cloud emission indicate that the density of the gas responsible for producing the ^{13}CO and CS emission must be substantially larger, suggesting that the density structure of the cloud is very inhomogeneous.

A number of facts about G216−2.5 suggest that it is in an evolutionary state between episodes of massive star formation. These facts include the relatively large velocity dispersion, the presence of shells and rings within the cloud, a velocity field which is dominated by a global velocity gradient, and the discrepancy between the LTE and virial masses. Finally, the striking similarities between G216−2.5 and Gem OB1-arc suggest that the two clouds are in a similar evolutionary state. Thus, we believe that G216−2.5 and Gem OB1-arc suggest that the two clouds are in a similar evolutionary state. Thus, we believe that G216−2.5 is a remnant cloud from a past episode of massive star formation; the progenitor star-forming complex may have included the S287 molecular cloud.

The Five College Radio Astronomy Observatory is operated with support from NSF grant AST91-15721 and with permission of the Metropolitan District Commision of Massachusetts. Y. L. is grateful to John Carpenter for providing Gem OB1 data, and to Mark Heyer and Taoling Xie for providing the image reduction package.

REFERENCES

Blitz, L. 1991, in The Physics of Star Formation and Early Stellar Evolution, ed. C. H. Lada & N. D. Kylafis (Dordrecht: Kluwer), 1
Blitz, L., Fich, M., & Stark, A. A. 1982, ApJS, 49, 183
Bloemen, J. B. G. M. 1987, in Interstellar Process, ed. D. J. Hollenbach & H. A. Thronson, Jr. (Dordrecht: Reidel), 143
———. 1989, ARA&A, 27, 469
Bloemen, J. B. G. M., Caraveo, P. A., Hermsen, Lebrun, F., Maddalena, R. J., Strong, A. W., & Thaddeus, P. 1984, A&A, 139, 37
Bohlin, R. C., Savage, B. D., & Drake, J. F. 1978, ApJ, 224, 132
Carpenter, J. M., Snell, R. L., & Schloerb, F. P. 1990, ApJ, 362, 147
——— 1992, private communication
Dickman, R. L. 1978, ApJS, 37, 407
Dickman, R. L., & Kleiner, S. C. 1985, ApJ, 295, 479
Dickman, R. L., Snell, R. L., & Schloerb, F. P. 1986, ApJ, 306, 326
Dodds, D., Strong, A. W., & Wolfendale, A. W. 1975, MNRAS, 171, 569
Erickson, N. R., Goldsmith, P. F., Novak, G., Grosslein, R. M., Viscuso, P. J., Erickson, R. B., & Predmore, R. 1992, IEEE Trans. MTT, 40 (No. 1), 1
Goldsmith, P. F. 1988, in Molecular Clouds in the Milky Way and External Galaxies, ed. R. L. Dickman, R. L. Snell, & J. S. Young (Dordrecht: Reidel), 1
Goldsmith, P. F., & Langer, W. D. 1978, ApJ, 222, 881
Green, S., & Thaddeus, P. 1976, ApJ, 205, 766
Higdon, J. C. 1979, ApJ, 113
Kutner, M. L., & Ulich, B. L. 1981, ApJ, 250, 341
Langer, W., Wilson, R. W., & Goldsmith, P. F. 1989, ApJ, 337, 355
Lebrun, F., Bennet, K., Bignami, G., Bloemen, J. B. G. M., & Buccheri, R. 1983, ApJ, 281, 634
Lee, Y. 1992, Ph.D. thesis, Univ. Massachusetts, Amherst
———. 1991, ApJ, 379, 639 (Paper I)
———. 1994, in preparation (Paper III)
Maddalena, R. J., & Thaddeus, P. 1985, ApJ, 294, 231
Mead, K. N., & Kutner, M. L. 1988, ApJ, 330, 399
Moffat, A. F. J., Fitzgerald, M. P., & Jackson, P. D. 1979, A&AS, 38, 197
Mooney, T. 1992, Ph.D. thesis, Univ. New York, Stony Brook
Myers, P. C., Dame, T. M., Thaddeus, P., Cohen, R. S., Silverberg, R. F., Dwek, E., & Hauser, M. G. 1986, ApJ, 301, 398
Neckel, T., Staude, H. J., Meisenheimer, K., Chini, R., & Gusten, R. 1989, A&A, 210, 378
Scoville, N. Z., & Sanders, D. B. 1987, in Interstellar Processes, ed. D. J. Hollenbach & H. A. Thronson, Jr. (Dordrecht: Reidel), 21
Scoville, N. Z., Yun, M. S., Clemens, D. P., Sanders, D. B., & Waller, W. H. 1987, ApJS, 63, 821
Snell, R. L. 1981, ApJS, 45, 121
Solomon, P. M., Rivolo, A. R., Barret, J., & Yahil, A. 1987, ApJ, 319, 730
Solomon, P. M., Sanders, D., & Rivolo, A. R. 1985, ApJ, 219, L19
Williams, J., & Blitz, L. 1993, ApJ, 405, L75